Article ID: 1003－6326(2004)01－0131－06

Correlation between microstructure and composition of Cu-In alloy①

ZHAO Cheng-zhi(赵成志), GUO Jing-jie(郭景杰), SU Yan-qing(苏彦庆),
WU Shi-ping(吴士平), JIA Jun(贾 均)
(School of Materials Science and Engineering, Harbin Institute of Technology, Harbin 150001, China)

Abstract: Four compositions of alloys were designed. They were Cu-2% In, Cu-7% In, Cu-11% In and Cu-23% In (mass fraction). These alloy specimens were prepared by metal mold. By means of microstructure observation, macrostructure observation and electron probe analyzing, microstructures and macrostructures of the specimens were analyzed by comparison method. Microstructure component and relationship between structure and composition of alloys were investigated. The results show that with increasing indium content, the grain changes from columnar one to equiaxed one, the equiaxed grain increases, the columnar grain zone decreases and the grain size becomes small. With increasing indium content, the growth way changes from planar one to dendritic one. Peritectic reaction plays inhibiting role on the growth of dendrite and affects the orientation of dendrite. Indium content has influence on lattice constant of Cu solid solution

Key words: Cu-In; mircrostructure; composition
CLC number: TG 111.4; TG 113.12 **Document code:** A

1 INTRODUCTION

As copper matrix materials are studied profoundly, and high and new technologies are used in materials research, their many new properties have been discovered, therefore the fields of their application have been extended continuously. Such as the development and application of shape memory alloy are according to the property of phase transformation of thermoelastic martensite[1]. These alloys include Cu-Zn-Al and Cu-Al-Ni ternary alloys, quaternary and quinary alloys derived from those two alloys, Cu-Mn-Al-Zn and Cu-Al-Ni-Mn-Ti[2]. Copper-tungsten alloys are used in electronic package material, which is according to the property of their low expansion coefficient and high heat conductivity[3]. In the field of electrical contact materials, the research of copper matrix materials becomes a prospect field due to their features of good properties and cheapness. The research fields focus mainly on Cu-Cr and Cu-W. The properties of Cu-Cr system materials are of high strength and high conductivity[4]. They are used in medium voltage and strong current vacuum circuit breaker and are studied profoundly[5-7]. The properties of Cu-W system materials are of high electric conductivity, high heat conductivity, strong electrical erosion resistance, strong fritting resistance and high strength[8]. They are used in high voltage vacuum contactor and breaker and are studied profoundly[9, 10]. The disadvantage of Cu-Cr and Cu-W system materials is their oxidizability in the atmosphere. Because the addition amount of alloying element is greater, the electric resistance of the materials is relatively greater. Cu-Cr and Cu-W system materials are formed by the method of powder metallurgy, and their processes are complex and the manufactural cost is high. The application of Cu-In and Cu-In system alloys in electrical contact materials are seldom reported. The selected composition range is in α phase region extended from 0 to 18.2% In, therefore, the addition amount of alloying element is less and the electrical resistivity of the materials is relatively smaller. The materials are mainly applied to photoelectric functional materials by adding together with selenium, sulfur and gallium. The alloys are in the state of film and are applied to solar battery. Their forming methods are elemental co-evaporation[11], spray pyrolysis[12] and electrodeposition[13-14]. As for Cu-In system alloy, their solidification, microstructure evolution and liquid-solid forming method have been seldom reported. Das et al[15] investigated the kinetics of eutectoid transformation in the Cu-In system, based on both the isothermal growth rate of the eutectoid colony and enthalpy changes during non-isothermal heating of solution-treated and quenched. They determined the maximum growth distance of the eutectoid cell and the equilibrium interlamellar spacing in the

① **Foundation item:** Project (JC-02-10) supported by the Science Fund of Heilongjiang Province for Distinguished Young Scholars
Received date: 2003－02－08; **Accepted date:** 2003－06－30
Correspondence: GUO Jing-jie, Professor, PhD; Tel: +86-451-86418415; E-mail: guojj@hit.edu.cn

temperature range of 600 ~ 825 K. They indicated that the eutectoid transformation in the Cu-In system was a boundary-diffusion-controlled process. Zahra et al[16] studied a crystallographic phase transition δ/γ at temperature of 905 K for γ phase with a composition of 29.6% In. They presented that the drop colorimetry measurements were used for the heat content between 298 K and 1 273 K and measured temperature and enthalpies of the transition δ/γ and fusion of γ/liquid. In this work, the specimens were prepared by casting, various compositions were designed and analyzed by comparison method, the structure evolution in solidification and the correlation between structure and composition of alloys were investigated.

2 EXPERIMENTAL

Charging materials consist of copper (copper content> 99.90%) and indium (indium content > 99.90%). Melting was performed in medium frequency induction furnace. Graphite was used to prevent them from oxidizing and deoxidize for oxidative melt in melting process. Four compositions of alloys were designed, and they have 2%, 7%, 11% and 23% In. The material of upper mold is copper, that of pedestal mold is steel. The sizes of specimens and the mold are listed in Table 1. The range number of the crucible is 3, and it consists of graphite and clay.

Table 1 Sizes of specimens and the mold (mm)

Specimen sizes			Outline dimension of mold and pedestal		
Width	Thickness	Height	Pedestal height	Upper mold	Pedestal
50	10	50	30	110	120

2.1 Experimental equipment

The experimental equipment includes medium induction furnace, mold, Olympus BHM-2UM vertical optical metallographical microscope, JEOL Superprobe 733 electron probe, HITACHI S-570 scanning electronic microscope, HP ScanJet 3400c scanning instrument, and so on.

2.2 Selection of metallographical specimens and observation section

Metallographical specimens were selected from specimens. Selected metallographical specimen is nearly equal to a quarter of the specimen. Metallograph was selected from the positions of top, center and bottom of metallographical specimen observation section, and these three positions correspond to the top, center and bottom position of the specimen when pouring. The macrostructure was scanned by HP ScanJet 3400c scanning instrument in order to observe macrostructure.

2.3 Metallographical specimen and its composition

Designed compositions and corresponding serial number of specimens are listed in Table 2.

Table 2 Chemical composition and heat number of specimens

Heat No.	w(In)/%
1	2
2	7
3	11
4	23

3 RESULTS AND ANALYSIS

3.1 Macrostructure analysis

The macro scanning images of the specimen are shown in Fig. 1. The left side of Fig. 1 corresponds to the top of the specimen and the right side of Fig. 1 corresponds to the bottom of the specimen. From Figs. 1(a) ~ (d), the indium content increases. It is found that the grain shape changes from columnar one to equiaxed one. The columnar grain zone reduces, the equiaxed grain zone increases and the grain size reduces.

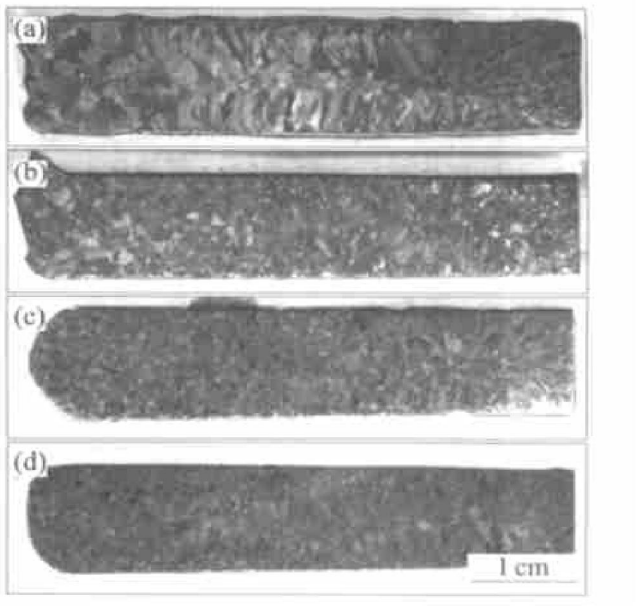

Fig. 1 Macrographs of specimens
(a) —Specimen 1; (b) —Specimen 2;
(c) —Specimen 3; (d) —Specimen 4

3.2 Microstructure analysis

Fig. 2 shows four microstructures taken from the same position of specimens. In Fig. 2(a), the growth way is cellular and the grain shape is irregular. The spot educts are the secondary phase δ_{II}. Figs. 2(b) and (c) are dendritic structures, and the dendrites are oriented. Light dendrites are primary α phase and dark structures among dendrites are δ phase. Fig. 2 (d) is dendritic structure. The length of primary and secondary dendrite arm is shorter

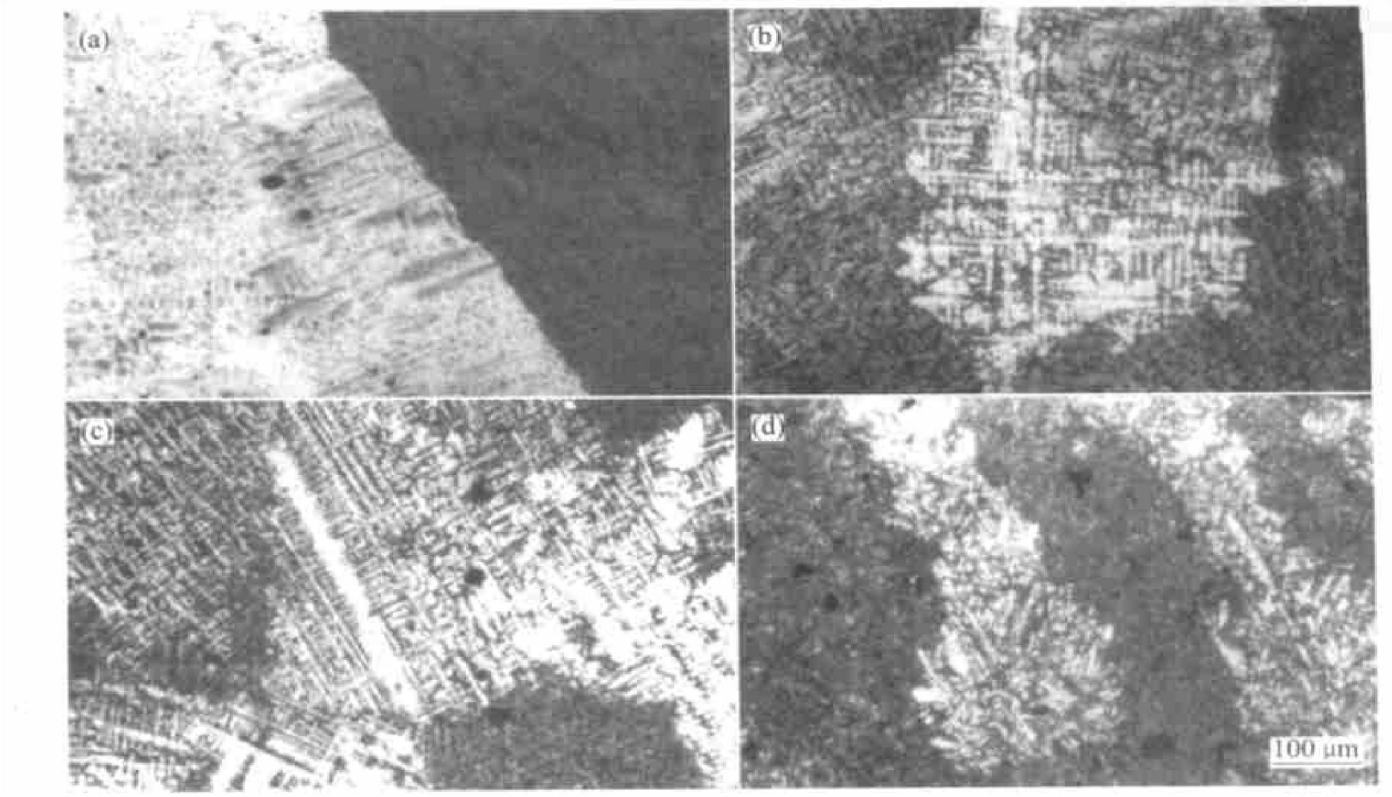

Fig. 2 Microstructures of four specimens at central positions
(a) —Specimen 1; (b) —Specimen 2; (c) —Specimen 3; (d) —Specimen 4

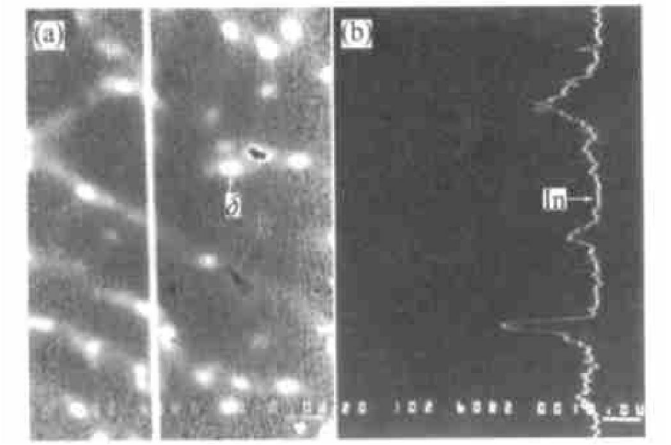

Fig. 3 Backscattered electron and line scanning image of Cu-2% In
(a) —Backscattered electron image;
(b) —Line scanning image

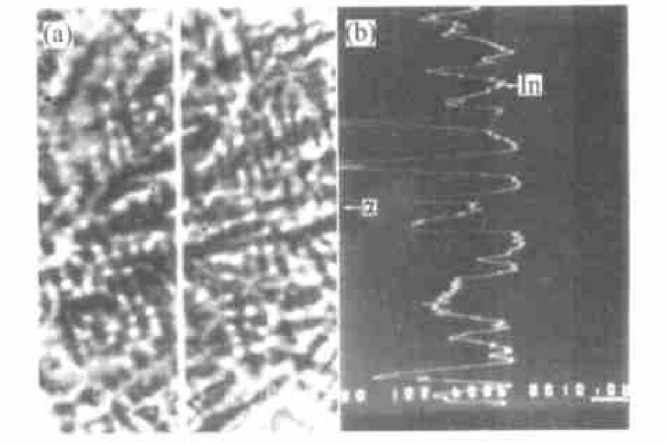

Fig. 4 Backscattered electron and line scanning image of Cu-11% In
(a) —Backscattered electron image;
(b) —Line scanning image

than that in Figs. 2(b) and (c), and the orientation of the dendrite is less obvious than that in Figs. 2(b) and (c).

Fig. 3 corresponds to Fig. 2(a), that is to say, the composition of both related specimens is the same. In Fig. 3(a), light spots are indium-rich phase that corresponds to the spots in Fig. 2(a), and it is δ_{II} phase. The curve in Fig. 3 is a line of indium distribution, which determines that the spots are indium-rich phase δ_{II}.

In Figs. 2(b) and (c), light dendrites are primary α phase. The microstructures both in Figs. 2(b) and(c) are similar. Fig. 4 corresponds to Fig. 2(c), therefore Fig. 2(c) can be used to analyze microstructure and constitution of phases in Figs. 2(b) and (c). In Fig. 4 (a), α dendrites are dark parts, corresponding to light dendrites in Figs. 2(b) and (c). δ phase is indium-rich phase and light spot in Fig. 4(a). It corresponds to the dark parts among dendrites in Figs. 2(b) and (c). The curve in Fig. 4(b) is line of indium distribution, which proves the analysis mentioned above.

Fig. 5 corresponds to Fig. 2(d) and Fig. 5(a) is the secondary electron image. The structures in Fig. 5 (a) are etched and consist of two parts: the light structures of convex parts and the dark structures of concave parts. The etching degree of the

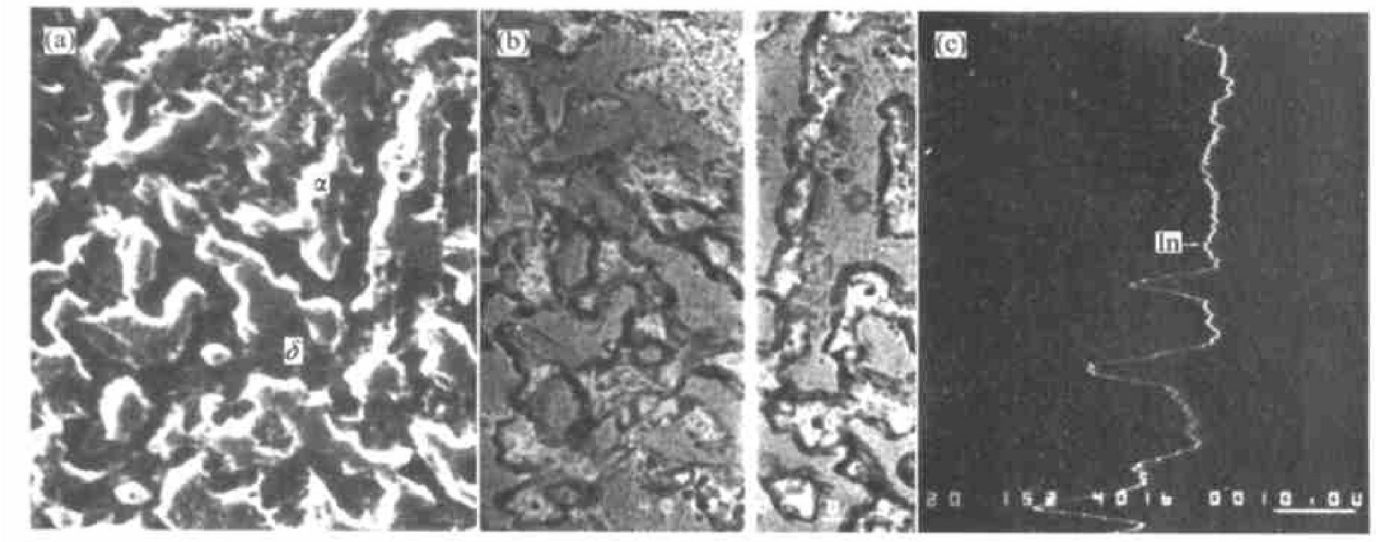

Fig. 5 Contrast of analysis image at same position of Cu-23% In
(a) —Secondary electron; (b) —Backscattered electron; (c) —Line scanning

former is thinner than that of the latter. The former corresponds to light α dendrites in Fig. 2(d) and the latter corresponds to dark δ phase among dendrites in Fig. 2(d). Fig. 5(b) corresponds to Fig. 5(a) and is a backscattered electron image. Light strips are indium-rich phase that corresponds to dark concave structures in Fig. 5(a). That is to say, the etching degree of indium-rich phase is deeper, therefore its surface is concave. In Fig. 5(b), the dark structures are copper-rich phase that corresponds to the light convex structures in Fig. 5(a). It shows that the etching degree of copper-rich phase is thinner. In brief, copper-rich phase is α phase and indium-rich phase is δ phase.

3.3 Analysis of phase composition and crystal structure

XRD tests were performed on the specimens. Fig. 6 shows the X-ray diffraction spectrum patterns of specimens. Figs. 6(a)~(d) correspond to alloys of Cu-2% In, Cu-7% In, Cu-11% In and Cu-23% In. All of their phase composition includes α phase and δ phase. But their phase contents are different. From Fig. 6(a)~(d), δ phase content increases.

The crystal of Cu solid solution is face-centered cubic structure. From the analysis results of X-ray diffraction, the parameters between the indium content and the interplanar distance are listed in Table 3.

Table 3 Interplanar distance d_{hkl}

w(In)/%	Indices of crystallographic plane				
	111	200	220	311	222
2	2.088 7	1.811 1	1.278 4	1.092 0	1.044 2
7	2.097 0	1.819 9	1.284 1	1.095 8	1.046 7
11	2.101 6	1.824 6	1.286 5	1.099 3	1.049 6
23	2.124 3	1.845 4	1.304 5	1.114 5	1.064 0

From the interplanar distance d_{hkl}, the lattice constants were figured out. The relation between the In content and the lattice constant a is shown in Fig. 7. From Fig. 7, it is seen that when the In content increases, the lattice constant also increases. That is because the radius of copper is 1.275, that of In is 1.57. The radius of In is greater than that of copper, therefore In atoms as solute replace copper atoms as solvent in crystal lattice, which causes lattice constant to become larger.

4 DISCUSSION

The compositions in Table 2 correspond to those in Fig. 8. The pouring temperatures, mold sizes, mold temperatures and environment temperature of specimens are approximate, therefore, it is assumed that the value of $G/\sqrt{v}$ is also approximate. As seen in Fig. 9[17], when the value of $G/\sqrt{v}$ holds constant and the value of w increases and the grains grow, the grain morphology changes from columnar one to equiaxed one. That is to say, the tendency to form equiaxed grain increases as w increases. This agrees with the results observed previously.

The same as above, as for four microstructures in Fig. 2, their conditions of solidification are close approximate, the position of selected metallograph is the same. It is considered that the value of expression $G/\sqrt{v}$ for four points of selected metallograph is approximate, where G is temperature gradient and v is solidification velocity. As seen in the images of the four microstructures, when composition w increases, the growth way of crystal changes from cellular to dendritic. This agrees with the relation between crystal morphology and three influencing factors[17]. As seen in Fig. 8 Cu-20% In, Cu-7% In and Cu-11% In

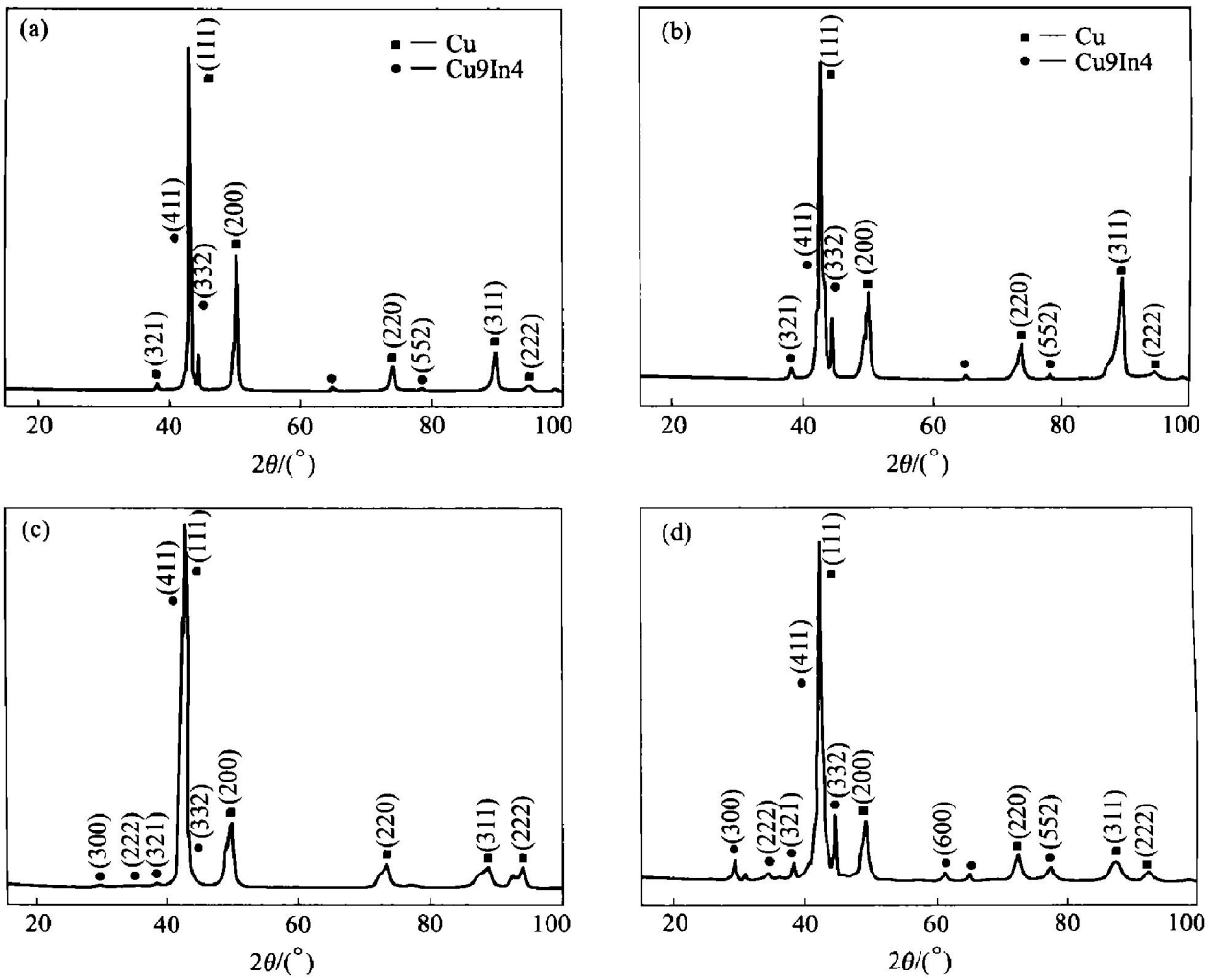

Fig. 6 X-ray diffraction spectra of specimens
(a) —Cu-2% In; (b) —Cu-7% In; (c) —Cu-11% In; (d) —Cu-23% In

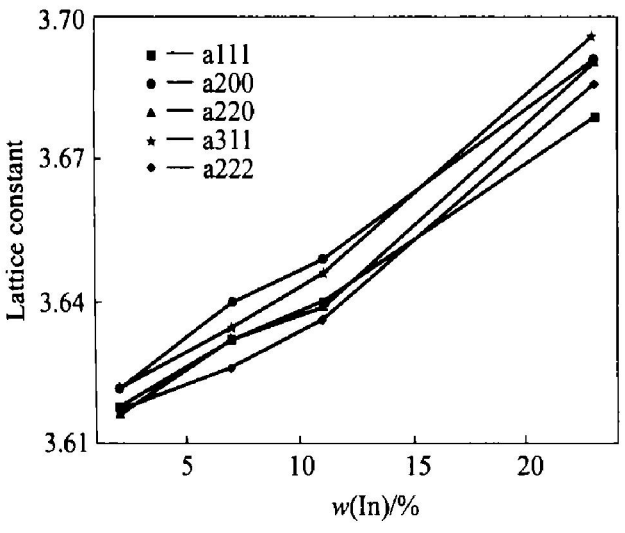

Fig. 7 Relation between lattice constant a and indium content

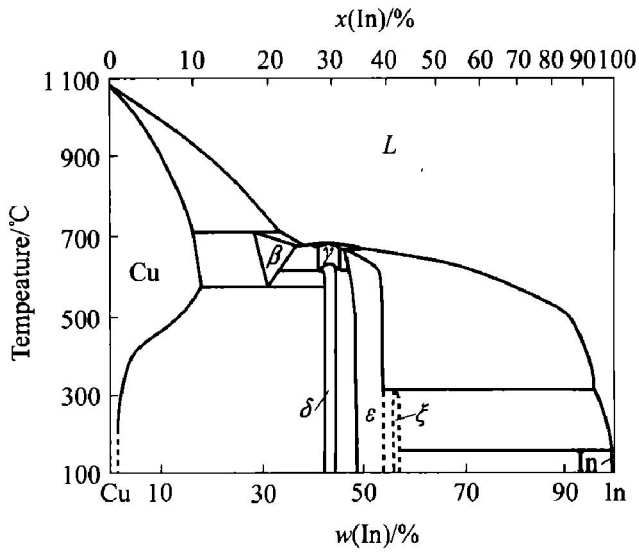

Fig. 8 Copper-In binary phase diagram

are solid solution alloys, while Cu-23% In is a product of peritectic and eutectoid reaction. As seen in Fig. 2, the dendritic orientations of Cu-7% In and Cu-11% In are more obvious than that of Cu-23% In, and the lengths of primary and secondary dendritic arm for Cu-7% In and Cu-11% In are longer than that for Cu-23% In. The reason is as follows: in process of dendrite growth, the solute content is higher; while primary grains grow, as seen in Fig. 8, the solute enriching at solidification front edge causes local liquidus temperature to drop and the degree of undercooling to decrease, which inhibits dendrite from growing and

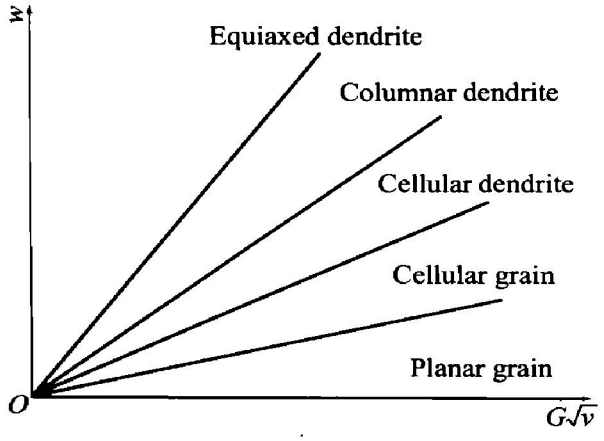

Fig. 9 Effects of $G/\sqrt{v}$ and w on morphology of crystal growth

affects dendrite orientation; on the other hand, due to peritectic reaction happening afterwards, β phase coats primary α phase, which inhibits dendrite from growing and affects dendrite orientation.

4 CONCLUSION

1) Microstructures of the Cu-In alloy can be divided into three types. The first one is Cu-2% In alloy, and their microstructure include α solute and spot δ phase; the second one is Cu-7% In and Cu-11% In alloy, and their microstructure includes α dendrites and spot δ phase, but their morphologies are different; the third one is Cu-23% In alloy, and their microstructure includes α dendrites and δ phase between dendrites.

2) The features of macrostructure are as follows: as the In content increases, the grain morphology changes from columnar one to equiaxed one and the columnar grain zone reduces and the grain size becomes small.

3) The In content has influence on lattice constant of Cu solid solution. When the In content increases, the lattice constant also increases and vice versa.

REFERENCES

[1] XU Zu-yao. Studies on phase transformations and their applications in materials engineering[J]. Heat Treatment, 2002, 17(1): 1-13.

[2] YANG Kai, GU Cheng-lin. Research and application of the shape memory alloy[J]. Metallic Functional Materials, 2000, 7(5): 7-12.

[3] JIANG Guo-sheng, WANG Zhi-fa, LIU Zheng-chun. Present status of the study on high-tungsten W-Cu composites[J]. Rare Metal and Hard Alloy, 1999(136): 39-42.

[4] CUI Yong-fu, SUN Xing-nan, ZHANG Jun. Properties of Cu50Cr50 contact material[J]. Rare Metal Material and Engineering, 1997, 26(5): 40-43.

[5] Li W P, Thomas R L, Smith R K. Effects of Cr content on the interruption ability of CuCr contact materials[A]. IEEE 19th Int Symp on Discharges and Electrical Insulation in Vacuum-Xi'an-2000[C]. 2000. 380-383.

[6] Spaic S, Komac M, Fetahagic A. Microstructure and properties of sintered Cu-25Cr alloy[J]. Materials Science and Technology, 1989, 5(11): 1069-1073.

[7] WANG Ya-ping, DING Bing-jun. The preparation and the properties of microcrystalline and nanocrystalline Cu-Cr contact materials[J]. IEEE Transactions on Components and Packaging Technology, 1999, 22(2): 467-472.

[8] Bregel T, Krauss-Vogt W, Michal R, et al. On the application of W/Cu materials in the fields of power engineering and plasma technology[J]. IEEE Transactions on Components, Hybrids and Manufacturing Technology, 1991, 14(1): 8-13.

[9] Raghu T, Sundaresan R, Ramakrishnan P, et al. Synthesis of nanocrystalline copper-tungsten alloys by mechanical alloying[J]. Mater Sci Eng A, 2001, 304-306(1-2): 438-441.

[10] JIA Cheng-chang, GUAN Xiu-hu, SU Xue-kuan, et al. Microstructure and properties of W-Cu alloys prepared with mechanically activated powder[J]. Journal of University of Science and Technology Beijing: Mineral Metallurgy Materials, 2001, 8(2): 129-132.

[11] Rockett A, Birkmire R W. CuInSe2 for photovoltaic applications[J]. J Appl Phys, 1991, 70(7): 81-97.

[12] Krunks M, Mikli V, Bijakina O, et al. Composition and structure of $CuInS_2$ films prepared by spray pyrolysis [J]. Thin Solid Film, 2000, 361-362: 61-64.

[13] Schaffler R, Klose M, Brieger M, et al. Pulsed laser deposition and characterization of CuInSe2 thin films for solar cell applications[J]. Mater Sci Forum, 1995, 173-174: 135-140.

[14] Sudo Y, Endo S, Irie T. Preparation and characterization of electrodeposited CuInSe2 thin films[J]. Jpn J Appl Phys, 1993, 32: 1562.

[15] Das A, Pabi K, Manna I. Kinetic of the eutectoid transformation in the Cu-In system[J]. Journal of Materials Science, 1999, 34: 1815-1821.

[16] Zahra B, Emma D, Bernard L. Heat Content and heat capacity of $Cu_{0.7}In_{0.3}$ from 298 K to 1 273 K[J]. Z Metallkd. 1999, 90(1): 55-59.

[17] HU Han-qi. Principles of Metal Solidification[M]. Beijing: Mechanical Industry Press, 2000. 127.

(Edited by LI Xiang-qun)